International Conference on Computational Methods in Marine Engineering
MARINE 2011
L.Eça, E. Oñate, J. García, T. Kvamsdal and P. Bergan (Eds)

USE OF RANS FOR ANALYSIS OF A HIGH-SPEED SEALIFT CONCEPT VESSEL

MARINE 2011

KEEGAN P. DELANEY

Naval Surface Warfare Center – Carderock Division
9500 MacArthur Blvd., West Bethesda, MD 20817 USA
e-mail: keegan.delaney@navy.mil

Key words: RANS, Multiphase, Powering, Waterjets.

1 INTRODUCTION

To better understand performance for high speed surface ships, Reynolds Averaged Navier-Stokes (RANS) calculations are performed on the Joint High Speed Sealift (JHSS), which is a monohull concept with four waterjets. The JHSS concept vessel is a long, slender hull form, approximately 290 m long with a beam of 32 m at full scale. Figure 1 shows the JHSS hull form and waterjet inlets. Both bare (without waterjet inlets) and powered (with waterjet inlets) hull forms are predicted and compared with experimental results documented in Cusanelli et. al. (2007). Computationally predicted quantitative features like sinkage, trim, resistance and thrust are compared to experimental measurements. In addition to the quantitative predictions, qualitative features like wave pattern and flow in and around the waterjet inlets are investigated.

Four model scale conditions are run in this study corresponding to a Froude number range of 0.24-0.40 (Reynolds number based on ship's length 19-31M). Table 1 shows a summary of full scale and corresponding Froude scaled model scale run conditions. All dimensions in this report should be assumed model scale unless otherwise specified.

Initially, the bare hull case is run using conformal structured grids at the experimentally determined fixed sinkage and trim to validate the RANS solver's multiphase capabilities. A grid dependency study is performed on the fixed bare hull case where the surface grid topology as well as refinement levels are varied. Next, computations are run for all four test speeds with the JHSS bare hull free to sink and trim to test the solver's motion prediction capabilities. The bare hull axial resistance, sinkage and trim predictions are compared to experimental measurements.

Lastly, the concept vessel is run powered with the waterjet inlets included in the model. The waterjet pump and shafts are not included in the model, instead a Body Force Propulsor (BFP) model is used to simulate propulsion by producing a pressure jump across a specified volume in the flow field. The waterjet inlet geometry is very complex, thus it would be very time consuming and computationally expensive to use a conformal structured grid for this geometry. Thus, powered computations use a Generalized Grid Interface (GGI) capability, which allows for non-conformal interfaces within the flow field. The GGI

capability allows for a structured mesh (hexahedral elements only) to be used around the free surface and most of the hull, and an unstructured mesh (prism and tetrahedral elements) to be used throughout the waterjet inlets. The predicted thrust from the BFP at the self-propulsion point from computations will be compared to experimental measurements.

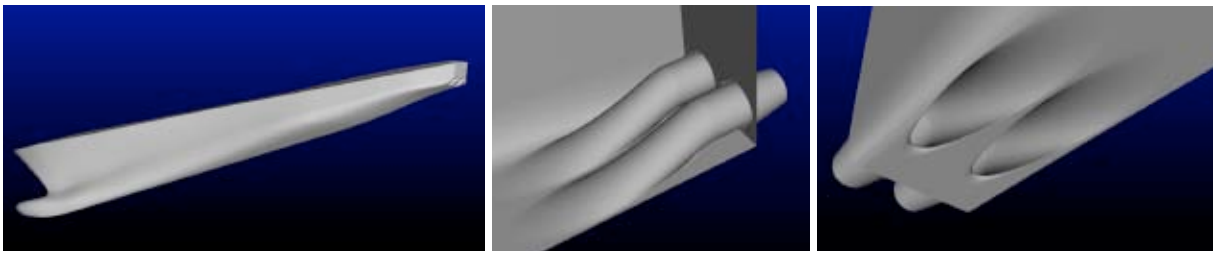

Figure 1: JHSS concept vessel (left), waterjet inlets from the top (middle) and from underneath (right).

Full Scale Speed (kn)	Full Scale Re	Froude Number	Model Scale Speed (m/s)	Model Scale Re
25	3,701 M	0.238	2.21	18.6 M
30	4,442 M	0.285	2.65	22.3 M
36	5,330 M	0.343	3.18	26.7 M
42	6,218 M	0.400	3.70	31.2 M

Table 1: JHSS full scale and constant Froude scaled model scale run conditions.

2 NUMERICAL METHODS

NavyFOAM V1.0's multiphase RANS solver is used for this work. NavyFOAM V1.0 (Shan *et al* 2010) was developed from the extended version of OpenFOAM (www.wikki.co.uk), which is extended from the standard release (www.openfoam.com). The solver employs a cell-centered finite-volume method that permits use of arbitrary polyhedral elements including quadrilateral, hexahedral, triangular, tetrahedral, pyramidal, prismatic, and hybrid meshes. The multiphase solver is run in parallel using domain decomposition and message passing.

For incompressible flows the continuity (mass conservation) and momentum equations can be written as Equations 1 and 2, respectively.

$$\frac{\partial U_i}{\partial x_i} = 0 \tag{1}$$

$$\frac{DU_i}{Dt} = -\frac{1}{\rho}\frac{\partial p}{\partial x_i} + \frac{\partial}{\partial x_j}\left(\nu\frac{\partial U_i}{\partial x_j} - \overline{u_i' u_j'}\right) \tag{2}$$

Where ρ is the density of the fluid, ν is the kinematic viscosity, p is the pressure, U_i is the mean velocity component and u_i' is the fluctuating velocity component. The term $\overline{u_i' u_j'}$ is the Reynolds stress. The Boussinesq approximation is used to relate the Reynolds stress to velocity gradients by Equation 3.

$$\overline{u_i' u_j'} = \nu_t\left(\frac{\partial U_i}{\partial x_j} + \frac{\partial U_j}{\partial x_i}\right) - \frac{2}{3}k\delta_{ij} \tag{3}$$

Where k is the turbulent kinetic energy and ν_t is the turbulent viscosity. Closure for the RANS equations is achieved by modeling ν_t using Menter's shear stress transport (SST) turbulence model, which is a two-equation k-ε/k-ω hybrid model (Menter 1994).

The Volume of Fluid (VOF) Method is used to locate and track the free surface (Hirt and Nichols). In the VOF method the volume fraction is advected throughout the domain according to Equation 4.

$$\frac{\partial \phi}{\partial t} + U_i\frac{\partial \phi}{\partial x_i} = 0 \tag{4}$$

Where ϕ is the volume fraction and varies from 0 to 1 for each cell depending on the percentage of each phase a cell contains.

3 GRID GENERATION

Both unstructured (prism and tetrahedral elements) and structured (hexahedral element) grids were used in this study. All grids were created with a non-dimensional normal wall spacing (y+) of ~40. Wall functions were used to reduce the number of boundary layer grid elements, thus expediting computations.

The commercial package Gridgen® was used for all structured grids. Bare hull computations used hexahedral elements only to retain accuracy around the free surface. Powered computations used a combination of hexahedral, prism, and tetrahedral elements, where the prism and tetrahedral elements are used to grid the waterjet inlets to ease gridding burden around the complex waterjet inlet geometries.

Multi-element unstructured grids were developed using SolidMesh (Gaither 1997), a suite of tools developed at Mississippi State University. SolidMesh provides tools for geometry preparation and surface grid generation. The volume grid is generated by using an advancing normal methodology for the boundary layer prism elements and an Advancing Front/Local Reconnection technique (Marcum and Gaither 1999) to develop isotropic elements.

4 BARE HULL RESULTS FOR FIXED SINKAGE AND TRIM

Initially, the bare hull is computed at fixed sinkage and trim model conditions. The computational model is fixed at experimentally determined design conditions (Froude number =0.343). A grid dependency study was done using two different blocking schemes for the bare hull. Figures 2 and 3 show the JHSS gridded using blocking scheme *A* and *B*. Grids *A* and *B* both contained ~2 million cells (taking advantage of wall functions) for the port/starboard symmetric half body. Additionally, a grid refinement study was completed on Grid *A*, where the grids tested range from 2-5 million elements for the half body.

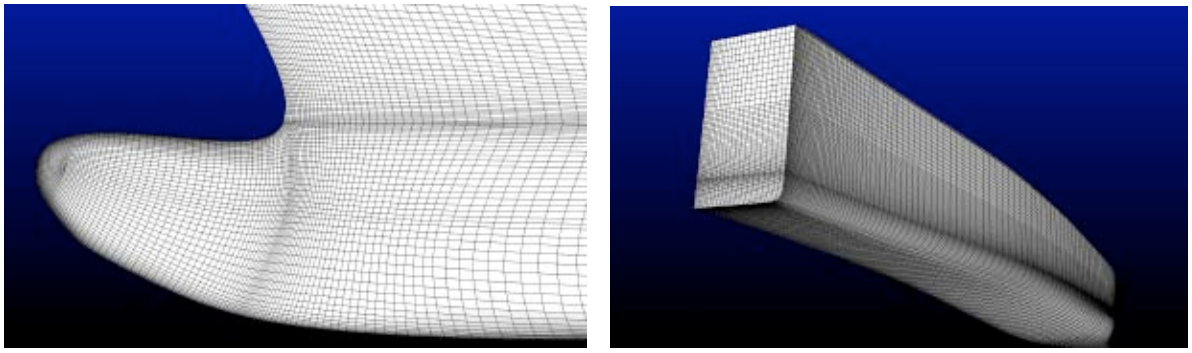

Figure 2: Surface mesh for blocking scheme *A* on the bow (left) and stern (right).

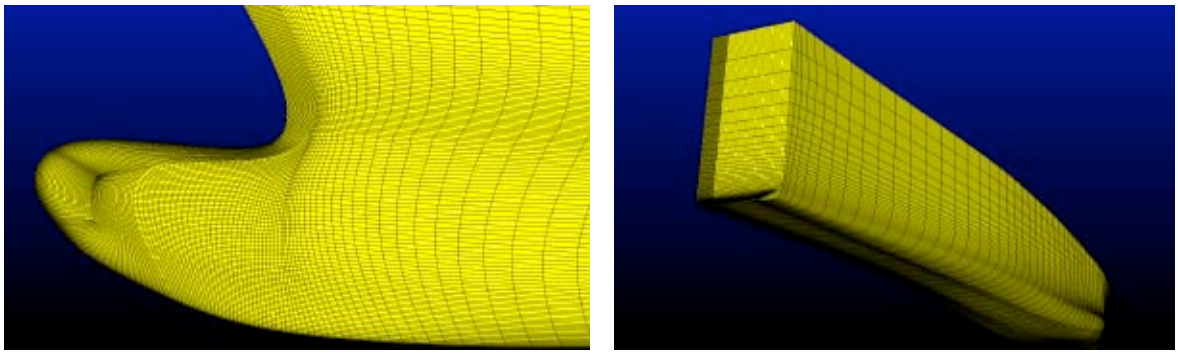

Figure 3: Surface mesh for blocking scheme *B* on the bow (left) and stern (right).

Figure 4 shows the wave profile on the hull for blocking scheme *A* and *B* baseline grids and the finest *A* grid. The computational results are also compared with experimental measurements taken by Cusanelli (2007). The experimental wave profile measurements were taken on the baseline shafts and struts JHSS configuration not the waterjet configuration; however, the hull forms are almost identical (same bow and midsection, and slightly different sterns). All of the computational results match experiment well with the exception of slight under resolution of the bow wave. The final grids used in this study use blocking scheme *A* with ~ 2 million cells for the port/starboard symmetric bare hull.

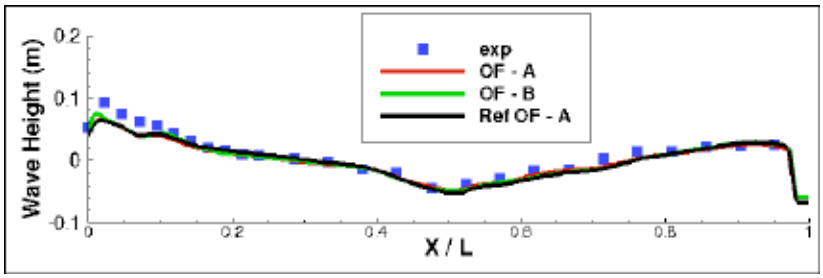

Figure 4: Wave profile on the JHSS hull from computation (OF-A, OF-B, Ref OF-A) and experimental measurement (exp).

Figure 5 shows the free surface results of the JHSS bare hull at fixed sinkage and trim. The disturbance of the free surface near the gooseneck bow is a result of minimal clearance between the bow and the undisturbed waterline. The Kelvin-like wave pattern around the midship and dry transom stern are also noticeable features of the JHSS at design conditions.

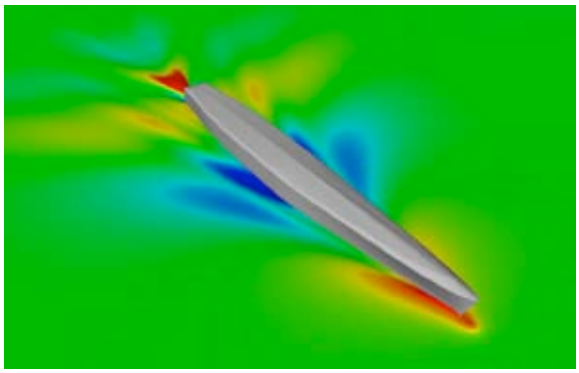

Figure 5: Wave pattern resulting from bare hull free surface computations. The free surface is colored by wave height.

5 BARE HULL RESULTS FOR FREE SINKAGE AND TRIM CONDITIONS

Next the bare hull is run free to sink and trim for all of the model scale conditions described above in Table 1. The computational model sinks and trims according to a rigid body mesh motion technique where the entire grid is free to move. The computations were marched forward in time until the ship's resistance, sinkage and trim oscillated minimally about a consistent mean. The plots in Figure 6 below show typical sinkage and trim progression throughout time for different model speeds.

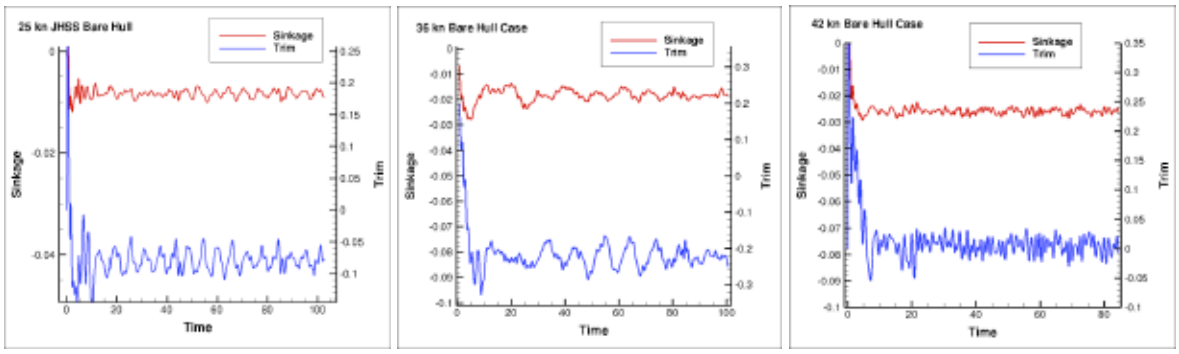

Figure 6: Sinkage and Trim plotted versus run time for 3 speeds.

Figure 7 shows the quantitative sinkage and trim results. The sinkage predictions match experimental results well, with a slight deviation at the highest Froude number case (the greatest difference is ~0.1% of the ship's length). The trim predictions also match experimental results well. The computational predictions correctly capture the bow down (negative trim angle) to bow up (positive trim angle) progression as the model ship speed is increased.

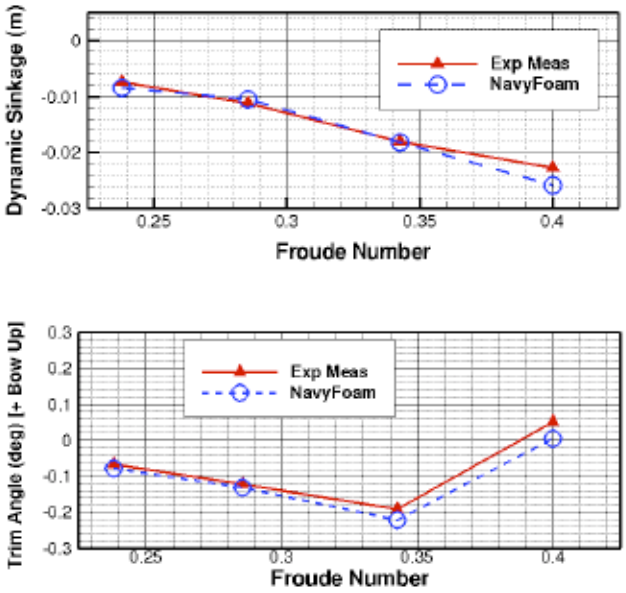

Figure 7: JHSS model sinkage and trim prediction for computation (NavyFOAM) and experimental measurements (Exp Meas).

Figure 8 shows the free surface colored by wave height for the JHSS bare hull at fixed sinkage and trim, and for the converged free to sink and trim case. Qualitatively the free surface predictions agree very well, which is expected as the predicted and measured sinkage and trim values agree well.

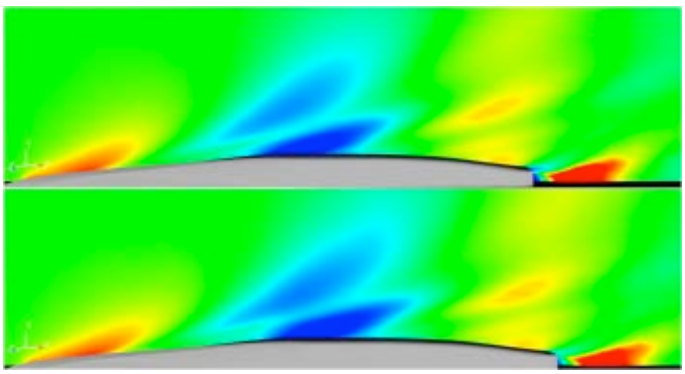

Figure 8: Fixed (top) and free to sink and trim (bottom) free surface plots colored by wave height at design conditions (Fr =0.343).

Figure 9 shows the total model resistance predicted over the Froude number range. Computational predictions and experimental measurements are nearly indistinguishable. There is less than 1.5% difference in computed and measured resistance at all tested run conditions. Correctly predicting the total resistance is an important statistic as in the traditional ship design process final full scale thrust at self-propulsion is determined from model scale total resistance (model resistance is scaled to full scale by the ITTC correlation line for frictional resistance and a constant wave making resistance assumption).

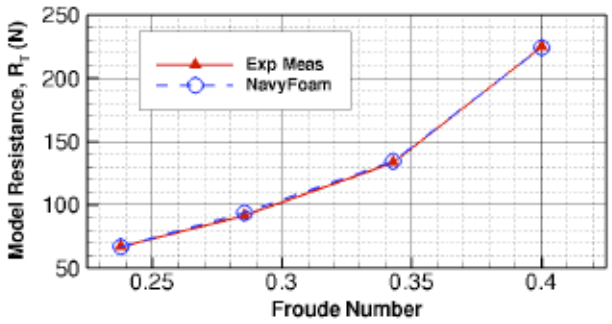

Figure 9: JHSS bare hull axial resistance RANS predictions compared with experimental measurements over a range of Froude Numbers.

6 POWERED RESULTS FOR FIXED SINKAGE AND TRIM

Finally, the powered model is run under fixed sinkage and trim conditions that were determined from experiment. The computational model includes the waterjet inlets, but the shafts, stators, and rotors are not included in the model. A previous JHSS powering study (Delaney 2009) has shown that it is not necessary to model the waterjet pump to get reasonable powering predictions. The effects of the waterjet pump are modeled by a Body Force Model.

As previously mentioned, the powering computations use both structured and unstructured grids in the same volume field, using GGI at the non-conformal interface. The structured portion of the grid (everywhere but waterjet inlets) uses the blocking scheme and spacing from the bare hull study. The surface mesh spacings and boundary layer growth rates for the unstructured grid used around the waterjet inlets was taken from the previous JHSS powering study (Delaney 2009).

Results of the powered computations through the non-conformal region can be seen in the streamwise cross sectional cut inside one of the waterjet inlets in Figure 10. Figure 10 shows the axial velocity is continuous across the non-conformal interface (unstructured inside the inlets and structured everywhere else) and the flow through the waterjet inlets behaves as expected, as the ingested boundary layer stays smooth through the transition regions.

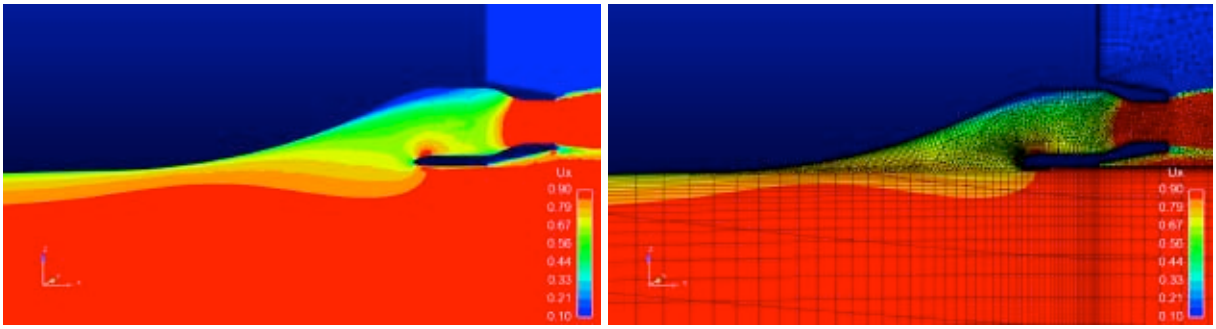

Figure 10: Axial velocity contours through the GGI interpolation region without (left) and with (right) the volume mesh overlayed.

The flow through the waterjet inlets involves extremely complex physics including interaction with the external free surface. Figure 11 qualitatively shows these features captured correctly as computationally predicted flow physics match photographs taken during the experiments. The transom stern is dry under model design conditions, and the water exits the waterjet inlets and interacts with the rooster tail coming up from underneath the hull.

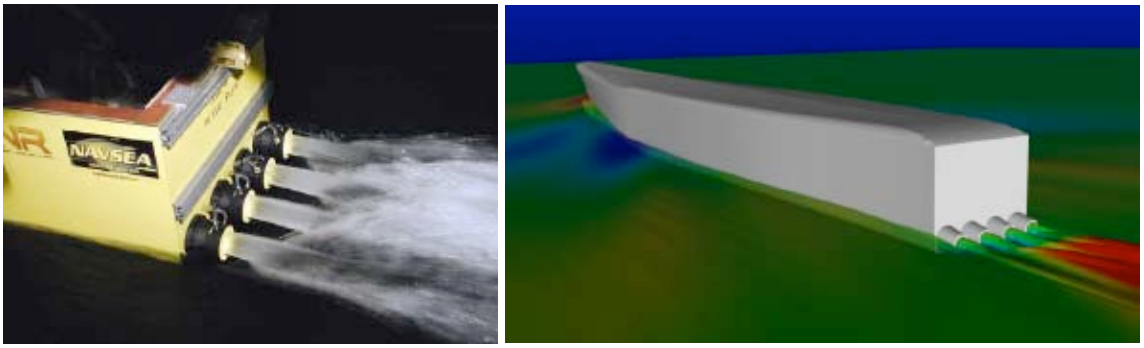

Figure 11: Aft view of the powered JHSS with water exiting the waterjet inlets and free surface colored by wave height.

For powering purposes the computational and experimental thrusts at self propulsion point are compared. It is important to note that there are differences in the way computed and experimental thrusts are determined. The computationally predicted thrust is determined as the thrust provided by the BFM that balances the model's resistance. It is not feasible to directly determine the experimental thrust from the waterjet pump. Thus, experimental thrusts are determined using the ITTC standard momentum thrust method (ITTC 1996) where the thrust is taken as the difference in momentum downstream and upstream from the the pump. The upstream momentum values are approximated from LDV measurements and assunptions about the shape of the streamtubes that are injested into the inlets. The downstream momentum values are determined from LDV measurements inside the inlets aft of the pump. The computed and experimental thrust predictions were 163 N and 153 N, respectively. The 6% difference in computed and experimental thrusts is reasonable considering the different techniques used to determine the thrust at self propulsion.

7 CONCLUSIONS

In conclusion, a computational study of the JHSS concept vessel hull form was completed. Computational results matched experimental measurements well for all test cases. Initially, a structured grid study was completed for the bare hull under fixed sinkage and trim conditions. A mesh was chosen from the grid study and used as the baseline for bare hull and powered computations. All of the meshes used in this study took advantage of wall functions, thus the cell count in the boundary layer was greatly reduced, resulting in less computational run time.

Bare hull computations showed that there was a slight under-resolution of the bow wave as compared to experimental measurements, which was most likely due to a combination of grid resolution and fidelity of the volume fraction convection scheme. Since completion of this work additional convection schemes designed for multiphase computations have been implemented in NavyFOAM and a comparison of these schemes for the JHSS could be a source of future work. Regardless, the slight under-resolution of the bow wave did not seem to significantly affect computed resistances.

Computations were also performed on the bare hull where the model was free to sink and trim. Computational sinkage and trim predictions matched experimental measurements well over a wide range of Froude numbers. Particularly, the bow down to bow up transition throughout the Froude range was successfully predicted. Also, the total resistance on the body matched experimental measurements very well for all Froude numbers.

Finally, powering calculations were run for the body at fixed sinkage and trim. The waterjet inlets were included in the geometry, but the actual pump was modeled by a Body Force Model. Also, a Generalized Grid Interface (GGI) capability which allows non-conformal interfaces in the flow field was used to combine structured and unstructured volume meshes in the same flow field. Many of the complex qualitative flow features around the waterjet inlets, like interaction of the rooster tail and flow exiting the waterjet inlets, were predicted correctly throughout the GGI regions. Quantitatively, computed thrust at self-propulsion was 6% different than experimental predictions, which is reasonable agreement considering the differences in computed and experiemental thrust determination. Powering

computations where the model is free to sink and trim were not a part of this study and could potentially be a source of future work.

ACKNOWLEDGEMENTS

This work was sponsored by Dr. Ki Han Kim from the U.S. Office of Naval Research.

REFERENCES

[1] Cusanelli, D., "Joint High Speed Sealift (JHSS) Baseline Shaft & Strut (Model 5653) Series 1: Bare Hull Resistance, Appended Resistance, and Alternative Bow Evaluations", Naval Surface Warfare Center Carderock Division Technical Report, NSWCCD-50-TR-2007/066, (2007).

[2] Cusanelli, D., Carpenter, S., and Powers, A.M., "Axial Waterjet Model 5662 and Mixed-Flow Waterjet Model 5662-1: Comparisons of Resistance and Model-Scale Powering with Propulsion Nozzle Designs", Naval Surface Warfare Center Carderock Division Technical Report, NSWCCD-50-TR-2007/076, (2007).

[3] Delaney, K., Donnelly, M., Ebert, M., and Fry, D., "Use of RANS for Waterjet Analysis of a High-Speed Sealift Concept Vessel", Proceedings of First International Symposium on Marine Propulsion, (2009).

[4] Gaither, A., "A Solid Modeling Topology Data Structure for General Grid Generation", Master's Thesis, Mississippi State University (1997).

[5] Hirt, C., and Nichols, B., "Volume of fluid (VOF) method for the dynamics of free boundaries", Journal of Computational Physics vol. 39 (1), pp. 201–225, (1981).

[6] ITTC, "Report of the Specialist Committee on Waterjets", 21st International Towing Tank Conference, Trondheim and Bergen, Norway, September 1996.

[7] Marcum, D., and Gaither, A., "Mixed Element Type Unstructured Grid Generation for Viscous Flow Applications", AIAA Paper No. 99-3252, (1999).

[8] Menter, F., "Two-Equation Eddy Viscosity Turbulence Models for Engineering Applications", AIAA Journal, Vol. 32, pp 1598-1605, (1994).

[9] Shan, H, Delaney, K., Kim, S-E., Rhee, B., Gorski, J., and Ebert,M., (2011), 'Guide To NavyFOAM V1.0.' NSWCCD-50-TR-2011/025, April 2011.